Photoinduced-Reaction Dynamics of Halogenated Alkanes on Iron Oxide Surfaces: CH_3I on $Fe_3O_4(111)-(2\times2)$†

G. G. Totir, Y. Le, and R. M. Osgood, Jr.*

Department of Applied Physics and Applied Mathematics, Columbia University, New York, New York 10027

Received: October 13, 2004; In Final Form: February 7, 2005

The adsorption, thermal chemistry, and photoreaction dynamics of methyl iodide on the (2×2) magnetite termination of natural single-crystal hematite have been investigated by time-of-flight quadrupole mass spectrometry (TOF-QMS), temperature-programmed desorption (TPD) and Auger electron spectroscopy (AES). The methyl iodide thermal desorption spectra, taken after dosing the (2×2) surface at 100 K with CH_3I, show a multiple-peak coverage-dependent behavior, consistent with the presence of several distinct adsorbed phases, along with defect-mediated dissociative chemisorption in the first monolayer. At >1 ML, methyl iodide forms a metastable physisorbed second layer, which desorbs at 148 K, but at higher coverage converts to a layer, which desorbs at 170 K. In the presence of low-fluence-pulse irradiation at 248 nm, angle-resolved TOF-QMS measurements show that 1.6 and 0.3 eV CH_3 fragments are ejected from the adsorbate surface; these fragments originate from direct photodissociation and dissociative photoinduced electron transfer, respectively. These energetic photoejected fragments have characteristic angular distributions peaked at ∼0° with respect to the surface normal. These results and the coverage-dependent relative intensities suggest that the predominant orientation in the first monolayer of the adsorbed CH_3I is normal to the crystal plane.

1. Introduction

The photochemistry of halogenated alkanes adsorbed on semiconductor or metal substrates has been studied extensively[1−7] both for a fundamental understanding of photoinduced bond cleavage and electron-transfer phenomena at surfaces, as well as for technological applications such as semiconductor etching,[8] environmental chemistry and remediation, photocatalysis, and photoelectrochemistry. The dynamics of photomediated processes in these adsorbate/substrate systems[1] are a result of several interrelated phenomena including: excitation by either photons or surface electrons and its dependence on the initial molecular and crystal degrees of freedom, loss of excitation to the surface via resonant or Auger-like processes, and perturbation of the isolated-molecule half-collision on the excited-state potential surface. The central advantage of employing ultraviolet-laser photoexcitation is its relative specificity for excitation of the adsorbed species compared to that by thermal excitation. In addition, the degree of excitation is sufficiently high so that large concentrations of fragments and other transient species can be prepared, thus allowing easy probing of reaction transients or products.

One important direction of research has been to examine the interrelation of orientation of the adsorbed molecular and photoexcitation dynamics. These studies have been extensively pursued on metals, insulators, and semiconductors in order to delineate reaction mechanisms for each of these surfaces.[2,5−7,9,10] This experimental work on orientation-resolved photochemistry has made effective use of angle-resolved time-of-flight mass spectroscopy and has observed striking phenomena such as site-specific chemistry and site-specific fragmentation, as well as their coverage and photon-energy dependence. Many of these studies have involved methyl halides or their higher alkane forms. For example, Stair and Weitz and their co-workers have investigated the photochemistry of methyl iodide on the wide-band gap oxides MgO and TiO_2[10−12] and showed that the photochemistry on these substrates was dominated by direct photodissociation, due to the absence of excited-state quenching in the presence of a wide band gap.

Alkyl halides were chosen as model adsorbate species for many of these studies because their excitation chemistry allows comparison of the two main dissociation processes that typically occur for these systems, namely, direct photodissociation (DD) of adsorbed species by incident ultraviolet radiation and dissociative electron attachment (DEA), which involves bond scission via attachment of low-energy photoelectrons generated in the substrate.[1−3,5] The competition between these processes is seen most on semiconducting surfaces such as GaAs(110), since its band gap is in an energy range, which enables excitation of surface photoelectrons at near-UV wavelengths.[5] In addition, the surface reconstructions on this well-known surface are well studied and are known to lead to orientation of molecular adsorbates.

In contrast to MgO and TiO_2, relatively few studies have been reported for small-band gap single-crystal metal oxides. These oxides can display unusual but useful properties for studies of surface-excitation chemistry, including, for example, a broad range of surface structure, variable surface conduction, and chemically labile surface lattice ions. In addition, because of their small band gap it is possible to readily excite surface photoelectron-based chemistry.

In this connection, the $Fe_3O_4(111)-(2\times2)$ selvedge formed on the (0001) plane of the α-Fe_2O_3 crystal has a small, i.e., ∼0.2 eV, band gap. It has also become the de facto model mineralogical substrate for reactivity studies with halogenated hydrocarbons. The chemistry of hematite and magnetite single-crystal specimens is relevant for various technological applica-

† Part of the special issue "George W. Flynn Festschrift."

* Corresponding author. E-mail: osgood@columbia.edu. Fax: (212) 860-6182.

10.1021/jp045326z CCC: $30.25
Published on Web 04/28/2005

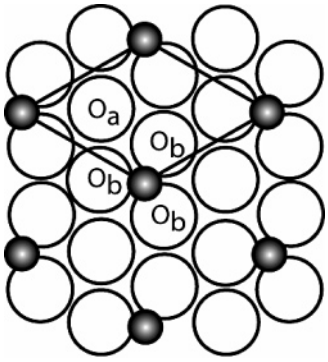

Figure 1. $Fe_3O_4(111)-(2\times2)$ surface ($a = 5.92$ Å). The oxygen atoms marked by O_b are capped by 1/4 of a monolayer of Fe^{3+} cations. The oxygen atoms marked by O_a are uncapped; in the bulk these coordinatively unsaturated oxygen atoms have a bond perpendicular to the plane of the surface. Image and terminology after ref 13b. The oxygen sites identified by O_a are likely to be abstracted.

tions, e.g., heterogeneous catalysis,[13] and for environmental catalytic processes, such as soil decontamination and organic-solvent remediation.[14−17] Single-crystal hematite, α-Fe_2O_3-(0001), has several different well studied surface reconstructions, which are obtained by varying the thermal annealing temperatures and oxygen partial pressures during the heating cycle. Previous research, including that using synchrotron, STM, and laboratory-based UHV probes, has shown that the three common terminations of reconstructed hematite surfaces, viz. magnetite, $Fe_3O_4(111)-(2\times2)$, hematite, $Fe_2O_3(0001)$, and the so-called "biphase", $Fe_2O_3(0001) + Fe_xO$, can display distinctly different reactivity toward different molecular adsorbates. Note that the "biphase" termination is a nanostructured superlattice of two crystallographic domains, namely hematite and wustite. A schematic representation showing the current understanding of the termination of the $Fe_3O_4(111)-(2\times2)$ surface is presented in Figure 1. This surface is terminated by 1/4 monolayer of tetrahedrally coordinated Fe^{3+} cations, which may act as strong Lewis acid sites. This termination results in 1/4 monolayer of the hexagonal closely packed surface oxygen atoms remaining uncapped by the surface iron atoms; these are identified as O_a in Figure 1.

In this paper we examine both the photochemistry and thermal chemistry of methyl iodide on the $Fe_3O_4(111)-(2\times2)$ termination of single-crystal hematite. Our TPD spectra show the formation of characteristic desorption spectra, which are similar to those seen on at least one other metal oxide surface. Our TOF measurements of CH_3 show velocity features characteristic of both the surface-reactions mechanisms mentioned above. Our angular-resolved measurements of the ejected methyl radical show that on the adsorbate molecular orientation the first monolayer of CH_3I on the (2×2) surface is consistent with the C−I bond lying in a direction parallel to the surface normal, with the CH_3 group projecting away from the surface.

2. Experimental Section

The experiments were conducted in a turbo-pumped UHV surface analysis system, which has a base pressure of approximately 3×10^{-10} Torr and is equipped with a retractable pinhole doser, an ion gun, an auger electron spectroscopy (AES) system, a LEED system, and a quadrupole mass spectrometer (QMS). The samples were α-Fe_2O_3 wafers, measuring $10 \times 10 \times 1$ mm^3, sliced from a naturally occurring single crystal and mechanically polished to a mirror finish to within 0.5° of the nominal (0001) plane (Commercial Crystal Laboratories, Inc.), as verified by back-reflection Laue X-ray diffraction. Prior to insertion into the UHV chamber, the crystals were cleaned in ethanol.

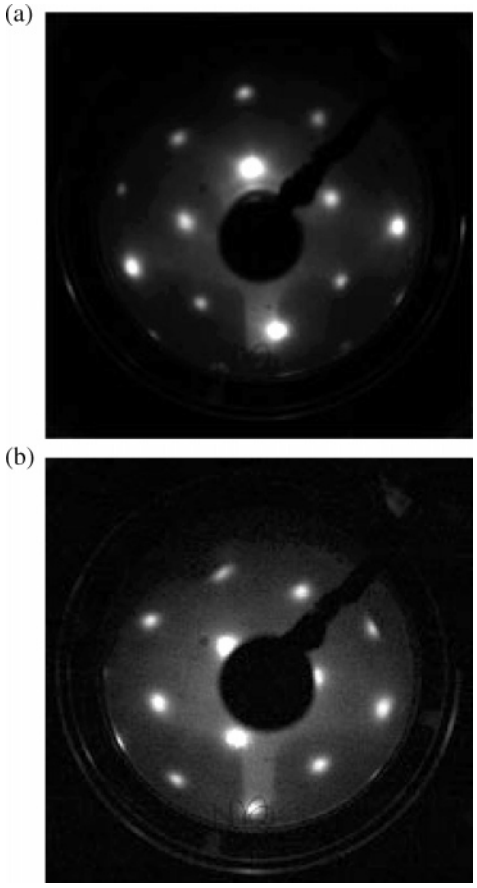

Figure 2. LEED images for the $Fe_3O_4(111)-(2\times2)$ surface: (a) unexposed sample after sputtering and annealing; (b) surface after thermal desorption of CH_3I, followed by annealing.

All experiments were carried out using the $Fe_3O_4(111)-(2\times2)$ termination formed on the (0001) plane of the α-Fe_2O_3 crystal. This surface was prepared by several cycles of Ar^+ sputtering at room temperature (2 kV beam voltage for 30 min with a 6 μA current through the sample) followed by multiple thermal annealing cycles. This Ar^+ sputtering causes preferential removal of oxygen from the near surface region, resulting in an amorphous surface as verified by the absence of LEED spots. Several 30-s thermal annealing cycles up to 1100 K were then used to restore surface crystallinity and form a chemically reduced surface-selvedge of $Fe_3O_4(111)-(2\times2)$ as verified by LEED, as shown in Figure 2a.

After surface preparation, the sample was cooled to 100 K and then exposed to CH_3I (99.5%, Aldrich) through a 0.1 mm diameter pinhole doser backfilled to 5 Torr. In the data below, all such exposures, under these conditions, are given in seconds. Using calibration data for exposure of other heavy alkanes in our system and assuming a constant, unity sticking coefficient for all cases (see discussion in **Section 3.1**), we estimate that ~1 L exposure (10^{-6} Torr·s) is obtained with a 60 s "dose". Prior to dosing, methyl iodide was purified by several freeze−pump−thaw cycles. Mass-resolved temperature-program-desorption measurements were made before and after UV irradiation exposure, to identify the reaction products and their characteristic desorption temperatures. All thermal desorption scans were performed using a computer-controlled linear temperature ramp of 2.5 K/s and the temperature readings were reproducible to within a few degrees. After each TPD measure-

ment, the samples were annealed to 1100 K for 30 s, to reestablish a clean well-ordered surface (see Figure 2b). The quality of this surface was ascertained by comparison of the CH_3I TPD spectra with that obtained from a sputter-annealed surface.

For TOF measurements, an excimer laser with 20-ns pulses was used at 10 Hz with a wavelength of 248 nm (KrF) and a fluence of ~0.3 mJ/cm^2 per pulse; thus all measurements were done using 248-nm-wavelength light. Operation at low laser powers prevented any significant laser-induced thermal desorption/reaction of the adsorbate. TOF measurements of the photofragments ejected from the surface into the QMS allowed for the determination of their kinetic energies. A synchronous pulse, from the laser, triggered collection of the digital output of the QMS by a multichannel scaler. TOF spectra for different detection angles were recorded by rotating the sample manipulator about the *z*-axis. During irradiation, the sample temperature was held at 100 K. After each irradiation, followed by post-irradiation TPD, each sample was cleaned by annealing to 1100 K for 30 s.

The velocity of the methyl fragments was determined by measuring the time-of-flight spectra at two distinct sample distances from the detector, obtained by precise translation of the sample along the same axis. For both measurements, the sample was carefully aligned first using a He−Ne laser until the central axis of the QMS matched the center of the working surface. The time difference between these two maxima was then used to convert the entire spectrum from time space to velocity space using a mass-spectrometer computer program previously described in ref 18.

3. Results

3.1. Adsorption of CH_3I on $Fe_3O_4(111)-(2\times2)$. Before surface irradiation at 100 K, thermal desorption spectra were recorded at different values of methyl iodide exposure or dose of the (2×2) surface. As shown in Figure 3a, four well-defined TPD features are observed at $m/e = 142$, i.e., CH_3I, over the temperature range from 140 to ~240 K; a magnified plot of these features is shown in Figure 3b, for the lower dose range. The relative magnitude of each of those features changes with exposure in progressing from submonolayer to multilayer coverage. The inset of Figure 3a shows a plot of integrated area under these TPD CH_3I spectra versus exposure in seconds; note that the curve is linear indicating that the sticking coefficient is constant with exposure. Thus, dose or exposure (in seconds) can be directly mapped into coverage in monolayers. As we will argue below, in our system a 45 s exposure yields ~1 ML coverage. The low desorption temperatures exhibited by these features along with the observation of similar features for adsorbed CH_3I on other single-crystal substrates[10−12,19−26] make it clear that these peaks can be attributed to desorption of the physisorbed molecules. In addition to these four major TPD peaks, a broad low-intensity desorption feature was observed at ~290 K even for at lowest CH_3I exposures; this feature had a long high-temperature wing extending to ~500 K. We attribute this feature to minority sites, i.e., defects on the magnetite surface.

We consider the four peaks as they appear with increasing dose or coverage. In presenting this discussion we use the notation adopted in ref 11, for studies of CH_3I on TiO_2 (see below). The highest-temperature nonminority feature, denoted as γ in Figure 3, was observed, for example, at ~240 K, for a 30 s dose. This peak saturated at a dose of 60 s and shifted down in temperature as the exposure increased toward this

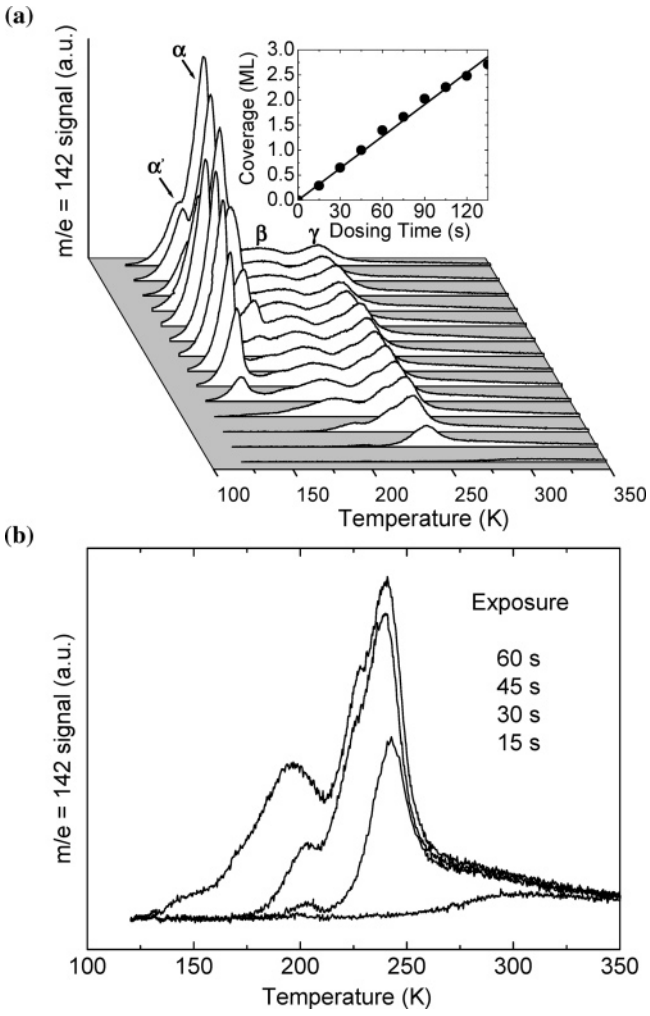

Figure 3. Temperature-programmed desorption (TPD) profile for CH_3I ($m/e = 142$) adsorbed on the $Fe_3O_4(111)-(2\times2)$ surface at 100 K as a function of coverage for exposures between 15 and 195 s: (a) coverage dependence set of "3D" TPD spectra for $m/e = 142$ (dose increases from front to back in the figure) and (b) the first four desorption curves at low coverage, magnified for clarity. The inset show measured total integrated TPD signal, i.e., coverage, vs exposure, or dose, in seconds from 0 to 120 s.

saturation dose (for a more quantitative discussion of this shift, see Section 3.2 below). A second thermal desorption feature, β, at 203 K was observed when the exposure increased to >30 s. With further coverage increase, the β peak position shifted only slightly toward lower desorption temperature until it stabilized around 194 K for doses higher than 60 s. As the dose was raised from 30 to 60 s, the peak area increased simultaneously for each of the two features, until saturation of the adsorbed features occurred at ~60 s exposure. This behavior suggests that γ and β features correspond to two different adsorption sites on the (2×2) surface, with limited surface migration of CH_3I molecules at temperatures below 200 K. For the 60 s saturation exposure, the β peak area is ~1/2 the area of the γ feature; see Figure 3. After taking into account the appearance and growth of the β TPD feature, as shown in Figure 3, and also after considering the correlation between dosing time and maximum peak intensity for the 240 K feature, we assigned a coverage of 1 ML to a 45 s CH_3I exposure.

For higher CH_3I exposures, a third desorption feature (α' in Figure 3) emerged at ~140 K (60 s dose) and grew in intensity as the dosing time was increased to 150 s. However, as the exposure was increased beyond 150 s, the intensity of this

desorption peak started to decrease, and a fourth desorption peak emerged at ~170 K (α in Figure 3). This fourth desorption feature continued to increase with exposure and eventually is dominant at >180 s CH_3I exposure. Since the peak 170 K peak did not saturate with increasing exposure, it originates from methyl iodide multilayers.

In summary, our measurements show two desorption features for the low-coverage (≤1 ML) regime and two for the multilayer regime; as discussed below those observations are consistent with others for CH_3I on oxide surfaces.

3.2. Thermal-Mediated CH_3I Dissociation of Methyl Iodide on the Single-Crystal Magnetite Surface. In addition to measurements of thermal desorption spectra for the molecular methyl iodide molecules on the (2×2) surface, TPD measurements were made for any reaction-generated products due to dissociative chemisorption of CH_3I on that same surface. In particular, our measurements used the $m/e = 127$ desorption peak, which corresponds to single-ionized iodine to provide insight into the interactions of halogen moieties with surface atoms. For desorption temperatures <300 K, the thermal desorption spectra using $m/e = 127$ are virtually identical to, and to some extent have better S/N ratio than, those obtained at $m/e = 142$, further indicating that these desorption features originate from molecular methyl iodide dissociated in the QMS. Note that these molecular spectra show the downward temperature shift of the γ peak, as the coverage increases from 0 to 1 ML, more clearly than seen in Figure 3. The temperature shift in the data of Figure 4a, is plotted separately in the inset to the figure.

In addition to this molecular desorption, a separate spectral feature was observed at much higher temperatures, i.e., >800 K. Figure 4b shows a series of coverage-dependent TPD spectra obtained for this high-temperature region. Only one thermal desorption peak is observed in this case, centered at 865 K. This iodine desorption feature achieves significant coverage at very low CH_3I exposure. For example, after only a 2 s dose, this 865 K TPD feature showed more than 50% saturation of its high-coverage value; see inset of Figure 4b. This behavior contrasts with the tendency observed for γ and β desorption features, which achieve complete saturation at much higher exposures, ~60 and ~75 s for the γ and β peaks, respectively. On the basis of an analysis of our mass 127 TPD data shown in Figure 4a (or 7b below) and using the procedure for estimating the relative ionization cross section of CH_3 and I described in ref 16, the degree of dissociation in the first monolayer of methyl iodide, in the absence of UV irradiation, was estimated to be <10%.

Because of the extremely small methyl iodide exposure times used here for investigating surface iodization, it was important to check for any potential experimental artifact arising from residual adsorbate in the UHV system and doser. Consequently, in a separate experiment, the freshly prepared clean sample was exposed for ~60 s to a previously filled doser, evacuated using the same procedure as in earlier runs, hence without allowing any intentional CH_3I vapor into the system. Subsequent TPD spectra showed no evidence of the $m/e = 127$ peak at 865 K. Finally, the presence of surface iodine was confirmed by separate Auger-electron spectroscopic (AES) measurements.

3.3. Photoinduced Reaction Dynamics. As mentioned above, methyl halides are useful model adsorbates for photodynamics experiments that study both direct dissociation (DD) by the incident ultraviolet radiation and dissociative electron attachment (DEA) by attachment of low-energy photoelectrons generated in the substrate. The competition between these two processes and its dependence on adsorbate coverage and wavelength has been demonstrated most clearly using semiconductors substitutes, since, while they have a substantial band gap, their work functions typically allow the ejection of surface photoelectrons at mid-ultraviolet wavelengths. A comparison of these two photodissociation channels is best achieved by probing the characteristic fragment kinetic energy for each of the above two processes. As a result, this section describes our time-of-flight (TOF) measurements recorded as a function of coverage and angle during irradiation of our CH_3I/magnetite surface system.

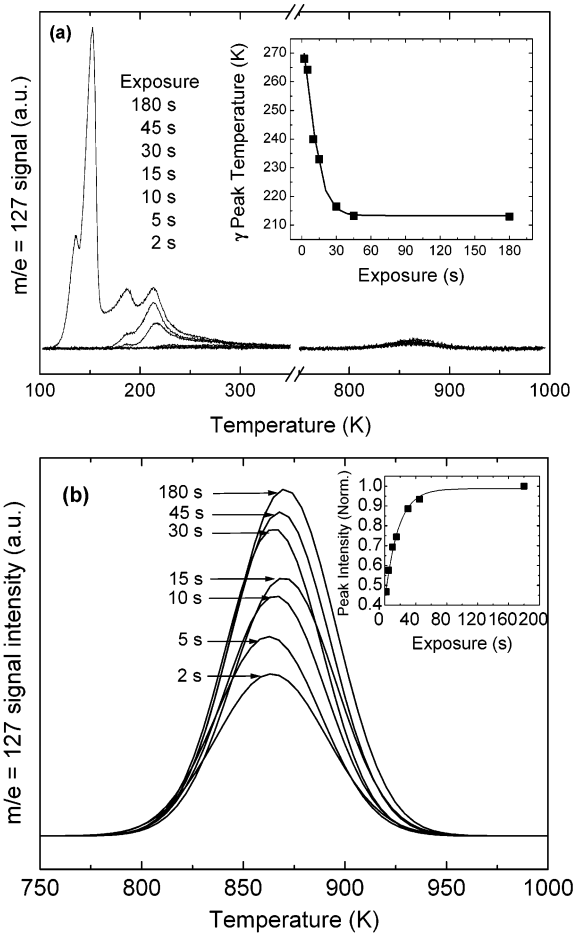

Figure 4. (a) Temperature-programmed desorption (TPD) profile for atomic I ($m/e = 127$) as a function of exposure between 2 and 180 s with an inset showing the temperature shift of γ peak. (b) Gaussian fit of the high-temperature (865 K) desorption peak with an inset showing the peak height of the $m/e = 127$ signal, normalized to its high exposure value.

The experiments consisted of irradiating the sample at a fixed and relatively low value of fluence and then observing the time-of-flight spectra of CH_3 both at a fixed angle, but variable coverage, and at a fixed coverage, but variable angle. The ejected CH_3 fragment was investigated since electron- and photon-mediated bond cleavage of methyl halides is know to occur at the carbon−halide bond and since, due to momentum conservation considerations, the lighter CH_3 fragment carries most of the translational energy after impulsive bond cleavage. To ensure that the adsorbed molecular layer was not depleted during UV irradiation, a series of time-of-fight spectra were measured as a function of UV irradiation time. In this experiment, a clean, characterized $Fe_3O_4(111)-(2\times2)$ surface was first dosed with ~1 ML methyl iodide, followed by successive exposures of 100 laser pulses at 0.3 mJ/cm^2. After measuring the change in the

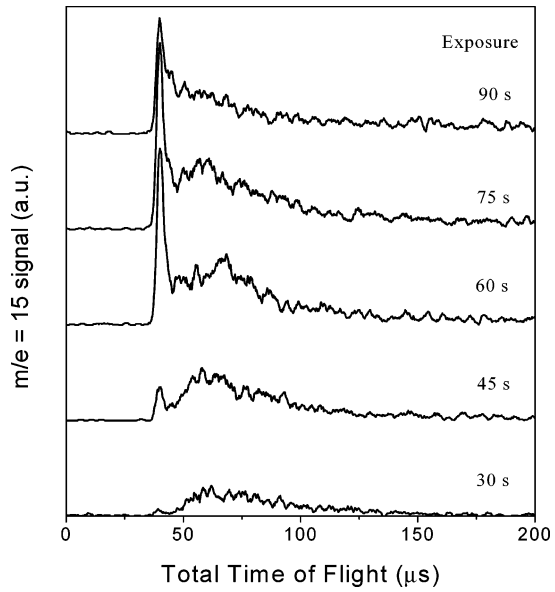

Figure 5. Time-of-flight (TOF) coverage-dependence for CH_3 (*m*/*e* = 15) signals as a function of coverage from submonolayer up to multilayer.

first monolayer TOF peak, it was determined that after each exposure to 100 shots the intensity of the TOF signal decreased by about ~10−15%. Thus, after a total sample exposure to 500 laser shots, the intensity of the low-energy TOF peak was ~50−60% of its original intensity.

3.3.1. Coverage Dependence of Time-of-Flight Spectra. Figure 5 shows a series of CH_3 TOF spectra obtained from 248 nm irradiation of the Fe_3O_4 sample after exposure to CH_3I doses ranging from 30 to 90 s i.e., from submonolayer to ~2 ML coverage. In general, two distinct velocity features are observed: a relatively narrow peak centered at ~40 μs arrival time and a much broader feature, corresponding to methyl fragments with lower velocities, centered at ~60 μs arrival time. Note that the arrival times for both peaks are constant within measurement error for all coverage. Using the procedure described in the Experimental Section, we measured a CH_3 velocity of 4800 m/s in the fast channel and ~2000 m/s for those in the slow channel, which corresponds to kinetic energy values of 1.6 and 0.3 eV, respectively.

The data in Figure 5 show distinct coverage-dependent behavior. At the lowest coverage, i.e., for a 30 s dose, the TOF spectra is dominated by the low-energy peak at 0.3 eV; the high-energy peak is present but with a low intensity. As the coverage is increased beyond 1 ML, ~45 s dose, the high-energy peak increases rapidly in intensity until it saturates between 1 and 2 ML. However, the low-energy peak has already begun to decrease in intensity at 1 ML and by 1.5 ML the integrated intensity of the high-energy peak is greater than that of the low-energy feature. At still higher coverage, the high-energy peak begins to decrease, and the low-energy feature is so low in intensity that its signal is overwhelmed by a featureless low-energy signal, which is most probably the result of scattered CH_3.

Our observations of the coverage dependence of the TOF measurements of CH_3 can be summarized as follows: the 0.3 eV channel is the predominant spectral feature at submonolayer coverage; only a trace signal is seen of the high-energy channel at the same low coverage. The presence of the high-energy peak for submonolayer coverage may indicate nonuniform monolayer formation, as discussed in more detail in Section 4. When the coverage exceeds 1 ML, the intensity of the high-energy channel increases dramatically. Our data also show that the low-energy channel saturates at a coverage of ~1 ML.

Our measured fragment kinetic energies are in good agreement with previous results obtained in our lab for CH_3 from methyl halides on GaAs(110). For example, TOF measurements performed in our laboratory for irradiation of 2 ML CH_3I on GaAs(110)[27] showed two separate fragment velocities: a sharp peak at 5500 m/s and a broad feature centered at about 3000 m/s, corresponding to energies of 2.3 and 0.7 eV, respectively. In our related measurements using REMPI-TOF probes, again using CH_3I on GaAs(110), two features were observed,[28] having kinetic energies of 1.6 and 0.3 eV, with generally the same coverage dependence for each as seen in the present work. In each of these studies, the features were identified as due to direct photodissociation and substrate-mediated dissociative electron attachment. These processes and their quenching, which is seen for coverage <1 ML, are discussed below in Section 4.

Photoreactions of gas-phase molecules at 248 nm have consistently shown that direct dissociation leads to the formation of both I and I*, that is, ground and spin-orbit excited iodine as well as CH_3. This same behavior has been shown in prior REMPI and TOF measurements of surface photoreactions, which also measured a yield of ~3 for I*/I.[4,7,9,28] The measurements were done either by directly measuring the flight time of iodine atoms or by inference from the velocity distribution of the ejected CH_3. In our experiments, which measured only CH_3 velocities, the S/N ratio was not sufficiently high to ascertain the presence of I; however, in several of our measurements showed indication of a weak signal at the TOF time expected for fragmentation into CH_3 and I.

3.3.2. Angle-Resolved Time-of-Flight Measurements. As discussed in the previous section, the velocity distribution of methyl fragments photoejected from the (2×2) surface is significantly different at high and low coverage. In these experiments, the angle-dependent TOF signals were measured on freshly prepared surfaces for a representative value of coverage in each of these two coverage regimes. Typically two sets of measurements were taken: one set at high CH_3I coverage and one at low coverage, corresponding to a dose of 60 s for >1 ML, and a dose of 30 s for <1 ML, respectively.

Angle-dependent TOF spectra for the 30 s dose are shown in Figure 6a, and spectra for the 60 s dose are shown in Figure 6b. As discussed in the previous section and shown in Figure 6, the dominant TOF feature at ~0° in the two coverage regimes is different: with the 1.6 eV feature being predominant at high coverage and the 0.3 eV feature dominant at lower coverage. However, as seen in Figure 6, the angular dependence of the TOF spectra shows the same general trends for both coverage regimes. Since the potential-energy curves of the isolated molecule are strongly repulsive near the equilibrium bond distance,[29] dissociation will be impulsive, ejecting CH_3 species in an angular distribution corresponding to the predominant molecular orientation of the adsorbed CH_3I.

These angular-dependent data can be quantified by fitting the 0.3 eV (DEA) and the 1.6 eV (DD) peak intensities, each with two distributions having a $(\cos\theta)^n$ dependence; these fitted distributions are shown for each of the two coverage regimes in the two insets in Figure 6a,b. In these cases, the exponent is not intended to be fit to that of a specific mechanistic model but rather to be used as an ad hoc measure of the sharpness of the angular lobe. In each case, the data correspond well to the two distributions, both centered on 0°, one with a sharp distribution having $n \gg 1$ and one with a broad distribution having n of O(1). We attribute this sharp distribution for both

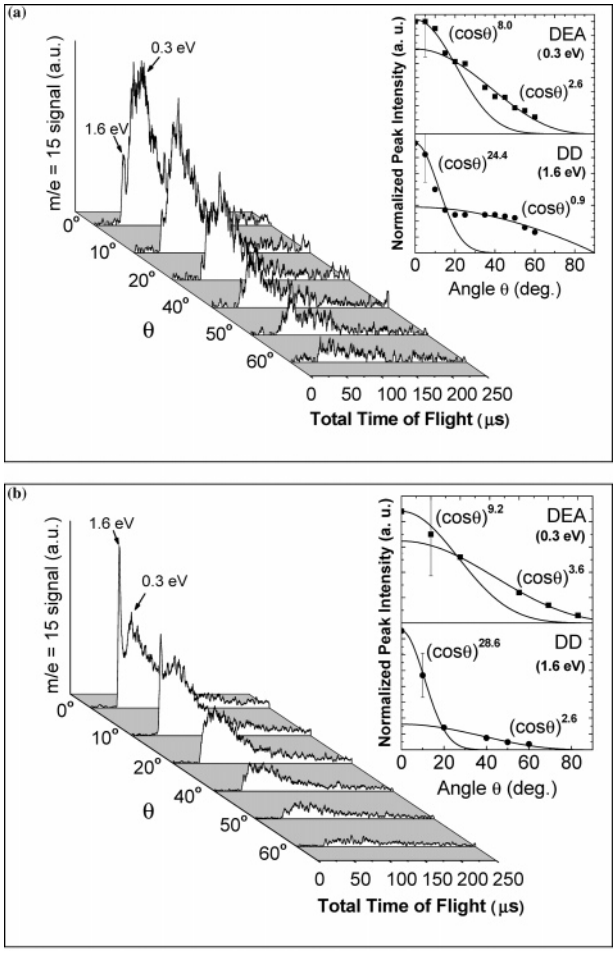

Figure 6. Measurements of angular dependence of the TOF spectrum for two distinct coverage regimes: (a) submonolayer (i.e. 0.67 ML) coverage and (b) >1 ML (i.e., 1.33 ML) coverage. The inset in each panel shows the measured peak intensity versus angle and a simple $(\cos\theta)^n$ fitting of the data. Because different mechanisms dominate each of these coverage regimes, the two panels allow comparison of direct photodissociation (DD) with dissociative electron attachment (DEA).

the 0.3 and the 1.6 eV cases to the primary, i.e., unscattered, fragments. In addition, we attribute the broad distribution to scattering due to imperfect adlayer order or substrate defects. Notice that the sharpest angular distribution is seen for fragments with the 1.6 eV fragment energy.

3.3.3. Postirradiation Thermal-Desorption Measurements. TPD spectra were recorded after low-fluence (~0.3 mJ/cm^2) irradiation of CH_3I dosed at 100 K on the (2×2) surface. Figure 7, panel a, compares the coverage dependence of thermal desorption spectra obtained for $m/e = 142$ without UV irradiation and after 500 pulses of 248 nm laser. One important observation is that the γ thermal desorption feature, which was observed at 240 K before irradiation, undergoes a greater reduction in intensity in the postirradiation spectrum as compared to other peaks. This behavior is seen most clearly in the 60 or 90 s data. Recall that the γ peak arises from absorption in the first monolayer on the (2×2) surface. Since these sites are specific to the (2×2) surface, they may be irreversibly blocked by surface photoproducts such as iodine atoms; this site poisoning would increase with irradiation time up to the point that all sites are blocked. This site blockage is different than that for the multilayer features, which are formed in the amorphous physisorbed films of pure CH_3I. The larger decrease in the γ peak compared to that in the other features, for the

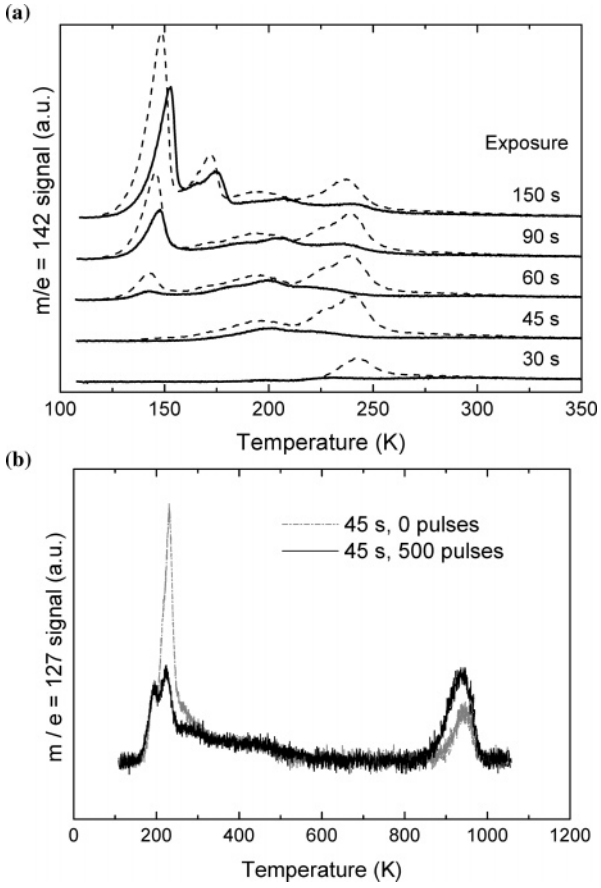

Figure 7. Postirradiation temperature-programmed desorption (PI-TPD) signals for (a) CH_3I ($m/e = 142$) and (b) I ($m/e = 127$) as a function of CH_3I dosing coverage after being exposed by incident 500 pulses of 248 nm laser irradiation.

same irradiation time, indicates a different photoreaction rate for the γ layer. Finally, in addition to the changes in the intensity of these molecular desorption peaks as shown in Figure 7, a broad post-irradiation TPD feature appears at ~540 K. This change is possibly due to the creation of new defect sites on the irradiated surface.

Postirradiation changes also occur in the high-temperature TPD feature for $m/e = 127$, corresponding to iodine. As seen in Figure 7b, the thermal desorption peak observed at ~860 K increases considerably after exposure of 1 ML CH_3I to 500 pulses of 248 nm laser. Since iodine may react with the lattice Fe, we also searched for any evidence of Fe in the mass spectra; no evidence of this species was seen, however. Thus this high-temperature feature must due to desorption of atomic iodine. These results indicate that methyl iodide, which is molecularly adsorbed in the first monolayer, undergoes photomediated bond cleavage, thus generating additional adsorbed iodine atoms. Note, that the high-temperature desorption peak shown in the upper curve was recorded after irradiation and represents the total accumulated signal both from surface iodine generated by thermal dissociation after the initial CH_3I dosing and from photogenerated iodine. Finally, these TPD results are in agreement with separate, complementary AES measurements performed on the same system. For example, these latter measurements showed an increase of ~10% in the iodine/oxygen Auger-peak intensity ratio after UV irradiation of ~10 ML of CH_3I.

In addition to changes in parent-molecular desorption, previous surface photochemistry studies have shown that UV irradiation of alkyl halides can lead to new chemical products formed from the "hot" methyl fragments.[19,21−24,26] To examine

whether these processes occurred in our system, measurements were made of any methyl reaction products at both high and low coverage of CH_3I. At low coverage there was no detectable thermal-desorption features for either CH_4 or C_2H_6, suggesting either that the chemistry of the CH_3 on the iron oxide surfaces is limited or, more likely (see below), that CH_3 is simply ejected from the surface following photoassisted bond cleavage. In contrast, for irradiation of >10 ML coverage surfaces, PITPD revealed that small amounts of both methane and ethane were detected. Specifically, the intensity of these $m/e = 16$ and 28 features appeared to increase approximately linearly with the methyl iodide dose. Since these features can originate from photodissociation within relatively thick multilayers, and hence they do not provide information on the photochemistry that occurs at the surface/adsorbate interface. These results are in agreement with previous data that showed the formation of both these alkanes after irradiation of multilayer methyl iodide on $Ag(111)$[26] and TiO_2.[19]

4. Discussion

4.1. Shifts in Desorption Temperature with Coverage. The results of our molecular CH_3I thermal desorption experiments are generally consistent with those obtained by others.[11] One of the most striking results of our measurements is the conversion of the high-temperature multilayer peak, α, into the low-temperature peak, α′, as the coverage increases into the multilayer regime. This formation of a metastable adsorbed layer followed by subsequent conversion into multilayer, as the coverage is increased, has been reported for a variety of substrate/ adsorbate systems, including aromatic compounds adsorbed on single-crystal metals.[30] In particular, the two multilayer peaks, α and α′, show virtually identical desorption temperatures to those in other CH_3I-substrate systems, using heating ramp rates close to ours. For example, Stair and Weitz and their and co-workers obtained desorption temperatures for α and α′ of 145 and 132 K in comparison to the values measured here of 152 and 136 K. Note that their heating rate (~3 K/s) was slightly higher than ours (2.5 K/s). This close agreement is expected since adsorption in the multilayer regime is decoupled from the substrate. Finally, Berko et al.[31] in their investigation of CH_3Cl on Pd(100) also observed very similar low-coverage TPD spectra as in our case; they showed that their spectra resulted from the formation of a discrete second layer, which is more weakly bound than the first layer, and thus it showed desorption kinetics that differ from the multilayer.

In addition, our two higher-temperature desorption features (γ and β) and their coverage dependence are consistent with the observations reported in ref 11. In particular, the β feature, within our measurement error, does not appear to shift when increasing the coverage from 0 to 1 ML. The γ feature exhibits a more substantial shift with coverage as is best seen by the TPD data for mass 127, where a 31 K change is observed increasing from 0.22 (244 K) to 1 ML (213 K) is seen. This value may be compared to a shift of ~37 K measured by Garrett et al.[11] over the same range of coverage. This shift is the result of dipole−dipole interactions, which change the adsorbate energy since the average molecular distance, and hence dipolar-repulsive interaction distance, varies with surface-site concentration. Finally note that, as expected, the two absolute "peak" desorption temperatures are different for the TiO_2 and the (2×2) surfaces since these features occur for adsorbed molecules in the first monolayer. Thus, for example, in our case the β peak is at 196 K while in the case of the TiO_2 surface it is at 155 K.[11]

Garrett et al.[11] argued that these two higher-temperature peaks, i.e., β and γ peaks of the $CD_3I/TiO_2(110)$ system, correspond to different adsorption geometries of the methyl iodide molecule or different adsorption sites. Such coverage-dependent changes in adsorbed-molecule orientation on dielectric surfaces have been discussed by others. For example, a recent study by Scoles and co-workers[32] concerning CH_3Br on single-crystal salt surfaces ascribed the coverage-dependent molecular orientation as follows: At low coverage, CH_3Br/ NaCl(001) is oriented such that the C−Br bond axis is nearly parallel to the surface plane, while at coverage close to 1 ML, the C−Br molecular axis in these adsorbate films is that of the surface normal as in the bulk-terminated $CH_3Br(011)$ surface. In addition, calculations by Guo et al.,[33] using the Monte Carlo method, made similar arguments for the CH_3Br and $CH_3I/LiF(001)$ system. Thus, it is reasonable that two phases, β and γ, should also be present in our data.

Finally, a Redhead analysis of the desorption temperature in our case gives a desorption energy of 0.57 eV for the 213 K peak, assuming first-order desorption kinetics, and a preexponential factor of 10^{13} s^{-1}. This value is close to the values seen on other crystal substrates. For example, a value of ~0.54 eV was measured for CH_3I on GaAs,[27] assuming a 10^{13} s^{-1} prefactor, or ~0.58 eV for CH_3I on Pt(111),[34] assuming a 10^{11} s^{-1} prefactor.

4.2. Time-of-Flight Dynamics. *4.2.1. Background.* As mentioned in the Introduction, the class of methyl halides has been a pervasive model system with which to investigate the surface-perturbed photochemical dynamics of molecularly adsorbed molecules. Several early studies on single-crystal metals[1,23] showed that, in general, for methyl halides, substrate-electron chemistry dominates at low coverage, i.e., $\theta < 1$ ML, while direct photodissociation dominates for $\theta \gg 1$ ML. At 1−2 ML coverage, either of these two processes results primarily in bond cleavage of the C−X bond and ejection of the alkyl radical. More recently, the photoreaction dynamics of methyl halides on insulating surfaces have been examined, including specific studies of methyl iodide. For example, Stair and Weitz and co-workers[9−12] studied photofragmentation of methyl iodide on MgO(100) and TiO_2(110). Using REMPI and angle-resolved TOF, they studied photochemistry of deuterated methyl iodide on these relatively wide-band gap oxide surfaces; for MgO-(100) and TiO_2(110), the bulk band gap values are 7.8 and 3 eV, respectively. Similarly, REMPI and TOF investigation of methyl iodide on NaCl and LiF[7,9] also showed that only direct photodissociative cleavage of the C−X bond occurred, at all coverage. Finally, photoreaction-dynamics measurements in our laboratories, including angle-resolved TOF and REMPI of CH_3I physisorbed on GaAs,[27,28] a medium band gap semiconductor, showed the presence of substrate-electron-mediated chemistry as well as direct photodissociation. The fragmentation in this case had strong angular lobes caused by preferential orientation of the adsorbed molecules coupled with strongly impulsive bond cleavage following either electron capture or photodissociation.

The general picture which emerges from this and other prior work is that UV surface photoreactions are the result of either direct dissociation (DD) or dissociative electron attachment (DEA), where the latter results from bond scission via attachment of low-energy substrate photoelectrons. The competition between these two processes depends strongly on adsorbate coverage and UV wavelength, and the optical and electronic properties of the substrate. Thus, direct photodissociation is strongly inhibited at low adsorbate coverage on metallic substrates[1] due to the efficient quenching of the excited state at

Angstrom-scale molecule/adsorbate spacing, which occurs by electron−hole pair formation. In contrast, for the top-layer molecules at high coverage or for insulators or wide band-gap semiconductors, only direct dissociation of adsorbed methyl-iodide molecules is observed.

The electronic properties of the natural hematite single-crystal used in our studies would allow photoelectron-attachment-type processes at low coverage. Specifically, the incident-photon energy of 248 nm (5.0 eV) used in these experiments exceeds the 2.2 eV band gap of single-crystal hematite, α-Fe_2O_3(0001), allowing excitation of hot carriers. Depending on the magnitude of the surface barrier, such carriers can tunnel into the unoccupied molecular orbitals of the adsorbed molecule. Adsorption of polar molecules such as CH_3I will increase this photoelectron flux since adsorption of methyl halides is known to lower the work function of certain substrate crystals.[3] Since all experiments described in this paper were performed on the "metallic" (2×2) surface, quenching of the directly photoexcited species by resonant electron excitation will occur as is seen on single-crystal metals. In particular, magnetite is generally described in the literature as having "metallic" conductivity,[15b] while a more quantitative calculation gives a band gap of no more than 0.2 eV for temperatures above the Verwey transition in Fe_3O_4.

4.2.2. Energetics. Our TOF flight data show two distinct CH_3 peaks, 1.6 and 0.3 eV, with the former being dominant at high coverage and the latter at low coverage. These translational energies are in accord with CH_3I photofragmentation data taken earlier using semiconductor and insulator surfaces. In particular, for wide band gap insulators, on which the high-energy methyl fragments are obtained by direction photodissociation, the photofragment energy has been found to vary to some degree with substrate.[9] In addition, our "TOF-peak" translational energy of 1.6 eV is in close agreement with typical values obtained in these earlier experiments. In addition, this energy agrees with measurements by our group of direct-photodissociatively ejected methyl radicals from >1 ML CH_3I on GaAs surfaces using REMPI-TOF measurements.[28] These same measurements also showed a lower-energy feature, i.e., 0.3 eV, which was due to fragmentation following dissociative electron attachment to CH_3I. In addition, the coverage dependence of this feature, that is, its predominance at submonolayer coverage, is also identical to that seen on GaAs. Thus, the measured energetics and coverage dependence allow us to identify these two mechanisms as occurring during 248 nm photoreactions on our iron oxide surface.

Note that in our TOF data, the 1.6 eV channel is seen, albeit at low intensity, even for coverage as low as 2/3 ML (30 s CH_3I dose). If we assuming that the direct dissociation photolysis pathway is indeed fully quenched for the first monolayer of adsorbed methyl iodide, the presence of a detectable signal for the high-energy channel at such a submonolayer dose would suggest the possibility that clustering or island formation occurs, rather than uniform layer-by-layer deposition. A similar surface phase has been reported previously in thermal desorption studies of methyl iodide Ag(111) by Zhou et al.[24] An alternate interpretation is that, unlike on semiconductors or metals, DD is not fully quenched in the first monolayer, perhaps due to more complex surface selvedge region.

4.2.3. Angular Dependence of Fragmentation. Previous studies of fragment angular distributions for physisorbed species have shown that at low irradiation flux and for strongly impulsive photodissociation events from 0 to 2 ML coverage surfaces, the distribution reflects primarily the orientation of the parent molecule prior to the dissociation event. This orientation depends on several factors related to the nature and structure of both the substrate material and the particular adsorbate species. For example, previous results obtained in this laboratory using halogenated alkanes on GaAs(110) and (100) have shown that these adsorbate molecules are oriented by local electrostatic forces with the surface Ga and As atoms; that is, the presence of ordered nanoterraces determines the orientation of adsorbed molecular dipoles on that surface.[5,6]

Our measurements here were directed heavily toward the dynamics of the methyl fragments; however, in earlier measurements on GaAs(110), we explicitly looked for ejected halogens both from brominated species and found that in the first monolayer, halogen fragments were only ejected "into" the semiconductor surface, where they form adsorbed halide products.[27] Recent STM experiments with CH_3Br on Si (7×7) have further confirmed this phenomenon.[35] The interpretation of our experiments here has also tacitly assumed that the majority of halogen atoms here are adsorbed at the surface.

The angular dependence of the ejected methyl fragments seen in our experiments exhibit, in all cases, a highly directional ejected CH_3 species exiting normal to the surface. In general, our angular orientation is most striking for the high-energy (1.6 eV) peak and at near or somewhat >1 ML coverage. More specifically, the angle-resolved TOF-QMS measurements indicate that the CH_3 fragments ejected at this coverage by bond cleavage have angular distributions, which are centered around ∼0° with respect to the surface normal. Since the potential-energy curves of the isolated molecule are strongly repulsive near the equilibrium bond distance,[29] dissociation will be impulsive; thus, the measured angular distribution suggests the predominant molecular orientation in the first monolayer of adsorbed CH_3I is normal to the crystal plane. For our (2×2) surface, it is reasonable to expect that CH_3I is adsorbed with the electronegative iodine oriented toward the uncapped surface Fe atoms. This result is consistent with the fact that studies of adsorbate-induced work function changes on metallic surfaces[3c] have indicated this same 90° halogen-on-metal orientation. It is also expected on the basis of simple chemical interaction between electronegative halogens and the nonfully coordinated Fe; thus, our earlier studies on the reactivity of halogenated hydrocarbons with Fe_3O_4(111)−(2×2) indicated a strong affinity of the lattice topmost Fe atoms toward halogens extraction reactions. The fact that low-coverage, i.e., <1 ML, layers give angular results with a large scattering component as we observe in Figure 6, is consistent with the fact that the molecular orientation will be less uniform on our surface at low coverage due to the greater importance of disorder from minority sites.

The larger angular lobe for the lower-energy electron-mediated fragmentation is consistent with earlier measurements using a series of alkyl halides with different chain lengths. In particular, wavelength-dependent studies[6] of fragmentation of methyl alkyls have shown that as the fragment energy becomes lower the directionality of the ejected alkyl ligands degrades. This behavior was attributed to the fact that lower fragment energies lead to greater angular width due to the increased importance of fragment-surface interactions during the half-collision.

Finally, our angular-dependent CH_3I measurements were confined exclusively to the monolayer-or-less-coverage regime, and as a result, the measurements presented here do not provide any indication of the presence of a directional ejection channel that would suggest a specific molecular orientation in the multilayer. However, we note that earlier NEXAFS measure-

ments by our group along with other TOF data[27] showed that in the case of CH_3Br/GaAs(110) second-layer molecules adsorbed in a direction to minimize dipolar energies; that is molecules formed alternating aligned layers as coverage increased.

4.3. Post-Irradiation TPD. Our TOF data is consistent with the preponderance of methyl fragments being ejected directly into vacuum following bond cleavage. Thus, it is not surprising that our postirradiation TPD showed no evidence of any photoinitiated surface-bound-methyl reaction products. In fact, only traces of both methane and ethane were observed after UV irradiation at very high coverage.

Photoreactions, which yield only fully ejected methyl species, have been reported before for alkyl halides on certain semiconductor surfaces. In those cases, the lack of secondary CH_3 reactions was a direct result of a highly ordered layer undergoing an impulsive reaction along the molecular axis such that the methyl species was ejected away from the surface. However, on metal surfaces more substantial evidence of secondary CH_3 reaction chemistry has been observed. These reactions have been found to follow a variety of possible mechanistic pathways, depending primarily on the substrate reactivity but also on the alkyl-chain structure. For example, White et al.[21] determined that CH_3 fragments formed via photodissociation of methyl iodide on Ag(111) recombine at the surface to form ethane, which was detected by postirradiation TPD. Similar results were obtained by Coon et al.[26] who measured substantial concentration of photoproducts generated from the irradiation at 248 nm of a much thicker layer ($\sim$70 ML) of methyl iodide on Ag(111). Note that photogenerated CH_3 chemistry for single-crystal Ag is different from observations on single-crystal Ni or Pt substrates, for which the predominant pathway reported was methyl dehydrogenation, leading to the formation of methane and molecular hydrogen.[21] Our case of CH_3I on iron oxide surfaces is apparently intermediate between those of GaAs(110) and single-crystal metals, since, in our case, only very small traces of ethane are seen. Unfortunately the larger number of surface defects present on our hematite surface may also play a role in the generation of higher hydrocarbons and, thus, a more definitive conclusion is not possible at this time.

5. Conclusions

In this paper, we have investigated the ultraviolet photochemistry of a methyl halide, CH_3I, on a small-band gap metal oxide surface. Since the UV photochemistry of this same species has been previously studied on other classes of substrate crystals, our experiments provide comparative data on additional type of substrate. Our results show that CH_3I has adsorbed phases, which are similar to those on other metal oxides, e.g., TiO_2, and thus displays similar thermal desorption spectra. In addition, its UV photochemical mechanisms resemble those on a medium band gap semiconductor and certain single-crystal metal surfaces; thus, measurement of the flight times from time-of-flight quadrupole mass spectroscopy shows that UV bond cleavage is a result of dissociative electron attachment at low coverage and direct photodissociation at a coverage >1 ML. Our angle-resolved measurements show that the adsorbate molecule is oriented with its carbon-halide bond along the surface normal. This orientation of the adsorbate molecule, along with the impulsive nature of either of the two possible reaction mechanisms, is consistent with the low level of secondary-methyl-reaction products seen in the thermal desorption data and the strong signal from ejected CH_3 fragments.

Acknowledgment. We gratefully acknowledge Drs. Nicholas Camillone III and Kaveh Adib of Brookhaven National Laboratory for several helpful discussions regarding our TOF data and instrumentation. In addition, we are pleased to thank Prof. George W. Flynn and Dr. Kwang T. Rim for many useful comments on the general subject of Fe_2O_3 surface chemistry. R.M.O. would like to thank George Flynn for years of professional discussions for inspiring the pursuit of a career in lasers and chemical physics. This work was supported by a DOE Grant (DE-FGO2-90ER14104), and instrumentation was funded by the Environmental Molecular Sciences Laboratory (NSF CHE-98-10367).

References and Notes

(1) Marsh, E. P.; Gilton, T. L.; Meier, W.; Schneider, M. R.; Cowin, J. P. *Phys. Rev. Lett.* **1988**, *61*, 2725.

(2) Ukraintsev, V. A.; Long, T. J.; Harrison, I. *J. Chem. Phys.* **1992**, *96*, 3957; Ukraintsev, V. A.; Long, T. J.; Gowl, T.; Harrison, I. *J. Chem. Phys.* **1992**, *96*, 9114.

(3) (a) Zhou, X.-L.; Zhu, X.-Y.; White, J. M. *Surf. Sci. Rep.* **1991**, *13*, 73. (b) Lin, M. C.; Ertl, G. *Annu. Rev. Phys. Chem.* **1986**, *37*, 587. (c) Jo, S. K.; White, J. M. *J. Phys. Chem.* **1990**, *94*, 6852.

(4) Yang, S. C.; Chen, J. M.; Wen, C.-R.; Hsu, Y. J.; Lee, Y. P.; Chuang, T. J.; Liu, Y. C. *Surf. Sci. Lett.* **1997**, *385*, L1010.

(5) Yang, Q. Y.; Schwarz. W. N.; Lasky, P. J.; Hood, S. C.; Loo, N. L.; Osgood, R. M., Jr. *Phys. Rev. Lett.* **1994**, *72*, 3068.

(6) Khan, K.; Camillone, N., III.; Osgood, R. M., Jr. *J. Phys. Chem.* **1999**, *103*, 5530; Khan, K.; Camillone, N., III.; Osgood, R. M., Jr. *J. Chem Phys.* **1999**, *110*, 10526.

(7) Jensen, E. T.; Polanyi, J. C. *J. Phys. Chem.* **1993**, *97*, 2257.

(8) Osgood, R. M., Jr.; Deutsch, T. F. *Science* **1985**, *227*, 709.

(9) Polanyi, J. C.; Sze, N. S.-K.; Wang, J.-X. *J. Phys. Chem. A* **1997**, *101*, 6679.

(10) Fairbrother, D. H.; Briggman, K. A.; Stair, P. C.; Weitz, E. *J. Phys. Chem.* **1994**, *98*, 13042.

(11) Garrett, S. J.; Holbert, V. P.; Stair, P. C.; Weitz, E. *J. Chem. Phys.* **1994**, *100*, 4615.

(12) Holbert, V. P.; Garrett, S. J.; Stair, P. C.; Weitz, E. *Surf. Sci.* **1996**, *346*, 189.

(13) a) Weiss, W.; Schlogl, R. *Top. Catal.* **2000**, *13*, 75; b) Joseph, Y.; Kuhrs, C.; Ranke, W.; Ritter, M.; Weiss, W. *Chem. Phys. Lett.* **1999**, *314*, 195.

(14) Peden, C. H. F.; Herman, G. S.; Ismagilov, I. Z.; Kay, B. D.; Henderson, M. A.; Kim, Y. J.; Chambers, S. A. *Catal. Today* **1999**, *51*, 513.

(15) (a) Myneni, S. C. B.; Tokunaga, T. K.; Brown, G. E. *Science* **1997**, *278*, 1106. (b) Brown, G. E.; Henrich, V. E.; Casey, W. H.; Clark, D. L.; Eggleston, C.; Felmy, A.; Goodman, D. W.; Gratzel, M.; Maciel, G.; McCarthy, M. I.; Nealson, K. H.; Sverjensky, D. A.; Toney, M. F.; Zachara, J. M. *Chem. Rev.* **1999**, *99*, 77.

(16) Adib, K.; Camillone, N., III.; Fitts, J. P.; Rim, K. T.; Flynn, G. W.; Joyce, S. A.; Osgood, R. M., Jr. *Surf. Sci.* **2002**, *497*, 127; Adib, K.; Totir, G. G.; Fitts, J. P.; Rim, K. T.; Mueller, T.; Flynn, G. W.; Joyce, S. A.; Osgood, R. M., Jr. *Surf. Sci.* **2003**, *537*, 191. Adib, K.; Mullins, D. R.; Totir, G.; Camillone, N., III; Fitts, J. P.; Rim, K. T.; Flynn, G. W.; Osgood, R. M., Jr. *Surf. Sci.* **2003**, *524*, 113.

(17) Camillone, N., III.; Adib, K.; Fitts, J. P.; Rim, K. T.; Flynn, G. W.; Joyce, S. A.; Osgood, R. M., Jr. *Surf. Sci.* **2002**, *511*, 267.

(18) Khan, K. A.; Moryl, J. E.; Slater, D. A.; Lasky, P. J.; Osgood, R. M., Jr. *J. Phys. Chem. B* **1997**, *101*, 9077.

(19) Kim, S. H.; Briggman, K. A.; Stair, P. C.; Weitz, E. *J. Vac. Sci. Technol. A* **1996**, *14*, 1557.

(20) Henderson, M. A.; Mitchell, G. E.; White, J. M.; *Surf. Sci.* **1987**, *184*, L325.

(21) Zhou, X. L.; White, J. M. *Chem. Phys. Lett.* **1987**, *142*, 376.

(22) Zhou, X. L.; White, J. M. *Surf. Sci.* **1988**, *194*, 438.

(23) Zhou, Y.; Henderson, M. A.; Feng, W. M.; White, J. M. *Surf. Sci.* **1989**, *224*, 386.

(24) Zhou, X. L.; Solymosi, F.; Blass, P. M.; Cannon, K. C.; White, J. M. *Surf. Sci.* **1989** *219*, 294.

(25) Lu, P. H.; Lasky, P. J.; Yang, Q. Y.; Wang, Y. B.; Osgood, R. M., Jr. *J. Chem. Phys.* **1994**, *101*, 10145.

(26) Coon, S. R.; Myli, K. B.; Grassian, V. H. *J. Phys. Chem.* **1995**, *99*, 16416.

(27) Lu, P. H.; Lasky, P. J.; Yang, Q. Y.; Osgood, R. M., Jr. *Chem. Phys.* **1996**, *205*, 143.

(28) Srivastava, A.; Osgood, R. M., Jr. *J. Chem. Phys.* **2003**, *119*, 10298; Srivastava, A.; Osgood, R. M., Jr. *Chem. Phys. Lett.* **2002**, *355*, 371.

(29) Black, J. F.; Powis, I. *Chem. Phys.* **1988**, *125*, 375.
(30) Huang, W. X.; White, J. M. *J. Phys. Chem. B* **2004**, *108*, 5060.
(31) Berkó, A.; Erley, W.; Sander, D. *J. Chem. Phys.* **1990**, *93*, 8300.
(32) Robinson, G. N.; Camillone, N., III.; Rowntree, P. A.; Liu, G.; Wang, J.; Scoles, G. *J. Chem. Phys.* **1992**, *96*, 9212.
(33) Huang, Z.-H.; Guo, H. *J. Chem. Phys.* **1993**, *98*, 7412.
(34) Panja, C.; Samano, E. C.; Saliba, N. A.; Koel, B. E. *Surf. Sci.* **2004**, *553*, 39.
(35) Dobrin, S.; Harikumar, R. K.; Polanyi, J. C. *Surf. Sci*. **2004**, *561*, 11.